

RubricRL: Simple Generalizable Rewards for Text-to-Image Generation

Xuelu Feng¹ Yunsheng Li² Ziyu Wan² Zixuan Gao³ * Junsong Yuan¹
 Dongdong Chen² Chunming Qiao¹

¹University at Buffalo ²Microsoft CoreAI ³Nikola Tesla STEM High School



Figure 1. Visual examples of our RubricRL on two language backbones. Equipped with interpretable and user-controlled criteria, RubricRL improves SFT models’ performance to generate high-quality images.

Abstract

Reinforcement learning (RL) has recently emerged as a promising approach for aligning text-to-image generative models with human preferences. A key challenge, however, lies in designing effective and interpretable rewards. Existing methods often rely on either composite metrics (e.g., CLIP, OCR, and realism scores) with fixed weights or a single scalar reward distilled from human preference models, which can limit interpretability and flexibility. We propose RubricRL, a simple and general framework for rubric-based reward design that offers greater interpretability, composability, and user control. Instead of using a black-box scalar signal, RubricRL dynamically constructs a structured rubric for each prompt—a decomposable checklist of fine-grained visual criteria such as object correctness, attribute accuracy, OCR fidelity, and realism—tailored to the input text. Each criterion is independently evaluated by a multimodal judge (e.g., o4-mini), and a prompt-adaptive weighting mechanism emphasizes the most relevant dimensions. This design not only produces interpretable and

modular supervision signals for policy optimization (e.g., GRPO or PPO), but also enables users to directly adjust which aspects to reward or penalize. Experiments with an autoregressive text-to-image model demonstrate that RubricRL improves prompt faithfulness, visual detail, and generalizability, while offering a flexible and extensible foundation for interpretable RL alignment across text-to-image architectures.

1. Introduction

Reinforcement learning (RL) has recently emerged as a promising approach for aligning generative models [3, 6–8, 21, 31, 32, 35–37, 39, 41] with human preferences. In large language models, frameworks such as RLHF [29] and RLVF [34, 55] have demonstrated that policy optimization guided by preference-based feedback can significantly enhance faithfulness, style, and usability. Extending this paradigm to text-to-image generation, including both diffusion and autoregressive (AR) architectures, offers a principled way to optimize models directly for human-aligned visual quality rather than likelihood-based objectives. However, the effectiveness of RL in visual domains critically

*Zixuan Gao contributed to this work during her research internship at the University at Buffalo.

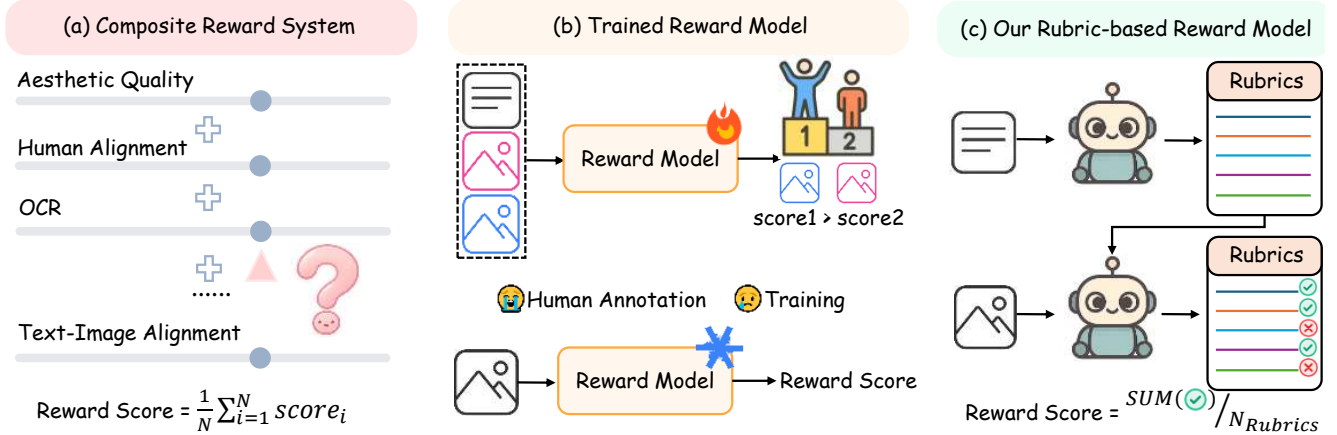


Figure 2. Comparison of RubricRL with prior autoregressive (AR) reward formulations. (a) Multi-reward pipelines combine CLIP, OCR, and realism metrics but require fragile weight tuning and often miss fine-grained attributes. (b) Unified scalar models collapse diverse objectives into a single learned score, simplifying optimization but reducing interpretability and adaptability. (c) RubricRL replaces both with a decomposable, prompt-adaptive rubric—an explicit checklist of visual criteria (counting, attributes, OCR/text fidelity, realism). Each criterion is scored independently and integrated into GRPO to provide interpretable, variance-aware supervision that improves detail, prompt faithfulness, and debuggability.

depends on reward design: constructing evaluation signals that are accurate, interpretable, and generalizable across prompts, domains, and architectures remains a core challenge.

Existing text-to-image RL frameworks can be broadly categorized into multi-reward mixtures and unified scalar reward models. Multi-reward systems (e.g., X-Omni [14], AR-GRPO [56]) combine heterogeneous objectives, such as CLIP-based image–text similarity [30], OCR accuracy [9], realism [51], and attribute consistency, to jointly encourage alignment and visual quality. While such approaches improve coverage, they depend on manually tuned weighting schemes that can be brittle across prompts and domains, and offer limited interpretability. Unified reward models (e.g., OneReward [15], Pref-GRPO [45], LLaVA-Reward [58]) instead learn a single scalar reward from pairwise human preference data. This simplifies optimization but can obscure the reasoning behind rewards, limit extensibility, and make it difficult for users to control which visual aspects are prioritized.

In this paper, we propose RubricRL, a simple and general framework for rubric-based rewards design in text-to-image models. Rather than relying on opaque scalar signals, RubricRL dynamically selects a structured rubric for each prompt, *i.e.*, a decomposable checklist of fine-grained visual criteria such as object correctness, attribute accuracy, OCR fidelity, compositional coherence, and realism. Each criterion is independently evaluated by a multimodal judge (e.g., GPT-o4-mini), while a prompt-adaptive weighting mechanism highlights the most relevant dimensions. This produces interpretable, modular supervision signals that integrate naturally into policy optimization frameworks such as GRPO [19] or PPO [33].

By expressing rewards in human-readable and decomposable form, RubricRL transforms reward evaluation from a black-box heuristic into an auditable process, where users can directly inspect, extend, or adjust which aspects of generation are rewarded or penalized. The rubric structure also facilitates per-criterion diagnostics, providing transparency into model behavior and simplifying both evaluation and debugging.

RubricRL is architecture-agnostic and compatible with both diffusion and autoregressive text-to-image models. The rubric outputs further support variance-aware group advantages, leading to robust updates even under long-horizon rollouts. Its prompt-adaptive design ensures that each reward vector reflects the salient aspects of the input text, such as numerals, named entities, styles, or embedded text, without requiring manual tuning.

We validate this simple yet effective idea using an AR text-to-image model. Experiments show that RubricRL improves prompt faithfulness, compositional accuracy, and visual realism, while maintaining high generalizability across datasets and architectures. Compared to prior multi-reward or unified-reward approaches, RubricRL achieves more consistent optimization behavior and enables controllable, interpretable reward shaping. Figure 1 provides visualization samples of our method, illustrating high visual quality.

In summary, RubricRL contributes:

- A generalizable rubric-based reward design applicable to both diffusion and AR text-to-image models;
- A prompt-adaptive, decomposable supervision framework that enhances interpretability and composability;
- A user-controllable and auditable interface that makes RL reward shaping transparent and easily extendable.

By operationalizing alignment through dynamically gen-

erated rubrics of explicit visual criteria, RubricRL makes reinforcement learning for text-to-image generation more interpretable, extensible, and user-guided, offering a unified foundation for aligning visual generation with human intent.

2. Related work

Text-to-Image Generation Methods. Text-to-image (T2I) generation has seen significant progress through both diffusion-based [5, 17, 28, 32, 48, 50] and autoregressive (AR) architectures [11, 49, 54, 57]. Diffusion models iteratively refine latent representations conditioned on text prompts, achieving high-quality and photorealistic images. Variants such as Stable Diffusion [32] and flow-based extensions [13, 26] provide diverse styles, controllable generation, and strong fidelity at both global and local levels. Autoregressive approaches, on the other hand, represent images as sequences of discrete tokens and model the joint distribution of text and image tokens using a single transformer backbone. Early hybrid designs, such as DreamLLM [11], paired AR text encoders with separate diffusion decoders. More recent unified AR models, including Chameleon [25], Emu3 [44], TransFusion [57], and Janus [49], integrate visual tokenization and autoregressive modeling in one architecture. These models allow direct mapping between text tokens and visual outputs, enabling flexible control and fine-grained generation. In this paper, we propose a novel reward design for reinforcement learning in text-to-image models, and demonstrate their effectiveness using a unified AR text-to-image model. However, our rubric-based rewards are applicable to both AR and diffusion architectures

Reinforcement Learning for Text-to-Image Generation. Maximum-likelihood training often under-optimizes user-salient qualities, such as semantic faithfulness, compositional accuracy, and aesthetics. Reinforcement learning (RL) offers task-aligned feedback that directly optimizes for human-relevant properties beyond likelihood. In diffusion-based text-to-image models, RL methods, such as Flow-GRPO [27], DanceGRPO [52], and reasoning-augmented T2I-R1 [24], have improved alignment by fine-tuning the generative policy with preference or metric-based rewards. Recently, RL has also been applied to unified AR T2I models [43], where policy gradients act directly on next-token probabilities, enabling end-to-end credit assignment and fine-grained control over generated images.

The design of the reward function is central to effective reinforcement learning in text-to-image models. One line of work aggregates heterogeneous signals—such as CLIP-based image–text alignment [30], OCR/text correctness [9, 47], multimodal VLM judges (*e.g.*, Qwen2.5-VL-32B [4]), aesthetic and realism metrics [53], and human-preference surrogates [51]. While comprehensive, these

multi-reward mixtures demand careful weighting and tuning, which can destabilize optimization and obscure per-aspect failures. Another direction trains unified preference models [45, 46, 58] to predict a single scalar human-aligned score from paired image outputs, simplifying optimization but relying on costly human annotations and limited scalability. In this work, we propose a rubric-based reward that is simple, generalizable, and interpretable. For each prompt, a compact rubric defines aspect-wise criteria—such as text alignment/OCR accuracy, object count, spatial relations, and overall coherence/quality. Each criterion is scored independently by a dedicated evaluator, and a transparent aggregation produces the final reward. This design is more prompt-adaptive, decomposable, and interpretable, while providing user-controllable and auditable feedback. While several concurrent works [18, 23] investigate rubric-based rewards in natural language processing, to the best of our knowledge, we are the first who proposes rubric based rewards in in text-to-image RL.

3. Method

In this paper, we use an AR based text-to-image model to verify the effective of our RubricRL framework, however it is generalizable to diffusion based model as well. This section starts by introducing the overall architecture of our RubricRL framework, followed by more details about the design of reburic based reward, RL training method and dynamic rollout sampling.

3.1. Overall architecture

As illustrated in Figure 3, given an input text prompt p , we first tokenize it into a sequence of text tokens, which are then fed into an autoregressive (AR) text-to-image generation model π_θ to predict a sequence of image tokens. These image tokens are subsequently decoded using a pre-trained, fixed VQ decoder to produce the final image I . In this paper, we primarily focus on post-RL fine-tuning of π_θ to further enhance its output quality, where designing an effective, reliable, and interpretable reward function is the key challenge. Existing methods typically employ one or multiple specialized models to evaluate different aspects of image quality, such as CLIP-based image–text semantic alignment reward [30] ($R_{\text{clip}}(I, p)$), OCR accuracy [9] ($R_{\text{ocr}}(I, p)$), and realism [51]. However, this approach has notable drawbacks: (1) deploying multiple specialized models is computationally expensive and difficult to scale to additional aspects; (2) it requires careful reward calibration and reweighting. Recent works have attempted to learn a single reward model from pairwise human preference data, simplifying optimization but offering limited extensibility due to high annotation costs and poor interpretability.

Motivated by the strong multimodal understanding ca-

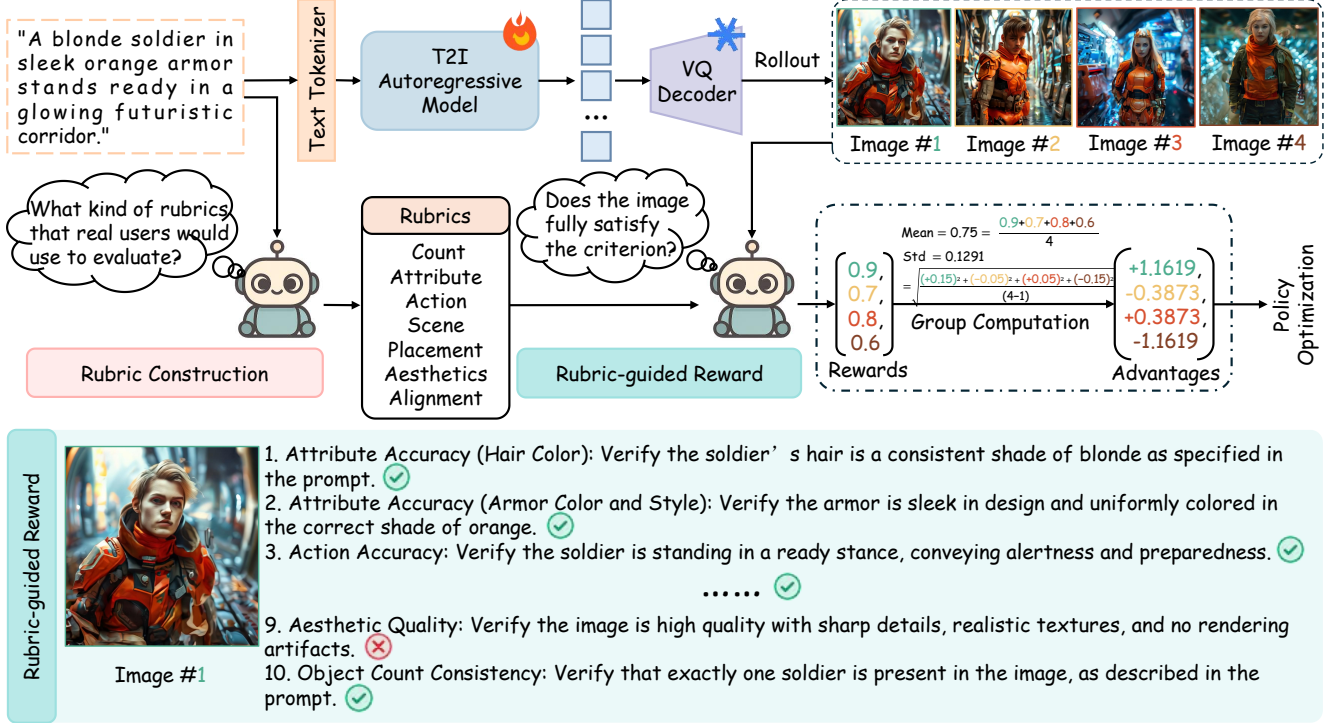


Figure 3. Overview of the proposed method. We propose a simple, general rubric generation pipeline and rubric-based reward model for unified text-to-image generation.

pabilities of modern multimodal LLMs such as GPT-5, we propose a simple and unified *rubric-based reward model*, denoted $R_{\text{rubric}}(I, p, \mathcal{C}(p))$. This model replaces the ensemble of task-specific evaluators with a single reasoning-capable vision-language model (VLM). Rather than relying on fixed sub-models, our approach automatically constructs a set of interpretable, prompt-adaptive criteria termed “*rubrics*” that capture the essential aspects of quality requirements for each specific prompt p .

In detail, given a text prompt p , a *Rubric Generation Model* \mathcal{G} (implemented via a large language model) generates a set of evaluation rubrics:

$$\mathcal{C}(p) = \mathcal{G}(p), \quad (1)$$

where $\mathcal{C}(p) = \{c_1, c_2, \dots, c_M\}$ defines M prompt-specific criteria encompassing dimensions such as object count, attribute accuracy, text/OCR fidelity, spatial relations, aesthetics, and style consistency. This ensures that the evaluation criteria dynamically adapt to the semantics and granularity of each input prompt.

In reinforcement learning (RL), the objective is to adjust the model parameters θ to maximize expected rubric based reward over the distribution of prompts:

$$\max_{\theta} \mathbb{E}_{p \sim \mathcal{D}, I \sim \pi_{\theta}(\cdot|p)} [R_{\text{rubric}}(I, p, \mathcal{C}(p))], \quad (2)$$

where \mathcal{D} denotes the set of prompts. A *rollout* corresponds to a single sampled image from π_{θ} given p , providing a re-

ward signal that guides policy updates. Compared to multi-model reward systems, our rubric-based formulation offers three key advantages: (1) **Simplicity**: it eliminates the need for multiple task-specific graders; (2) **Adaptivity**: rubrics are dynamically generated for each prompt, ensuring relevance to diverse user intents; and (3) **Interpretability**: each reward component corresponds to a human-readable evaluation criterion, enabling transparent model diagnostics and controllable optimization.

3.2. Rubric based reward

The rubric based reward function proceeds in two stages. First, a *Rubric Generation Model* \mathcal{G} interprets the user prompt p and produces a set of candidate evaluation rubrics $\mathcal{C}(p)$. Second, a multimodal LLM grader implements the *Rubric-Based Reward* $R_{\text{rubric}}(I, p, \mathcal{C}(p))$ that scores a generated image I against each rubric in $\mathcal{C}(p)$. In this paper, we employ GPT-o4-mini to fulfill both roles, generating prompt-specific rubrics and providing per-criterion judgments that are aggregated into a scalar reward.

Rubric construction. Given a user prompt p , we ask GPT-o4-mini to generate a list of rubrics. Each rubric entry contains a short eval key that targets a specific aspect (e.g., OCR alignment, object count, spatial relations, aesthetics) and a concise description of what to check in the image.

To promote diversity and reduce positional bias during rubric generation, we randomly permute the evaluation as-

pects in the rubric generation prompt and query GPT-o4-mini multiple times. In each round, the model produces a set of rubrics (we request 10 per query; because a prompt may describe multiple objects or attributes, the model may output multiple rubrics for one eval key to ensure adequate coverage). We aggregate all valid key–criterion pairs across runs into a unified rubric pool, discarding ambiguous or malformed entries. Finally, to remove redundancy and focus on the most important signals, we ask GPT-o4-mini to choose the top-10 most relevant and critical criteria for evaluating images generated from the user prompt p .

Rubric-guided reward. Given a generated image I , its corresponding text prompt p and the rubric pool \mathcal{C} , we simply ask GPT-o4-mini again to output a single score $y_i \in \{0, 1\}$ for each criteria to reflect whether the generated image fully satisfies this rubric ($y_i = 1$) or not ($y_i = 0$). The overall rubric reward is computed as the normalized mean of:

$$R(I, p, \mathcal{C}) = \frac{1}{M} \sum_{i=1}^M y_i, \quad M = 10 \quad (3)$$

3.3. Reinforcement learning with GRPO

To align the autoregressive image generator with rubric-based rewards, we employ **Group Relative Policy Optimization (GRPO)** [34], a variant of PPO designed for stable optimization over grouped rollouts. For each prompt, the set of generated rollouts forms a group, and the reward of each rollout is normalized relative to the group to reduce variance and improve credit assignment. Concretely, let π_θ denote the current policy and R_i the rubric reward for rollout i in group g . GRPO computes the relative advantage

$$A_i = \frac{R_i - \bar{R}_g}{\sqrt{\frac{1}{|g|-1} \sum_{j \in g} (R_j - \bar{R}_g)^2}}, \quad \bar{R}_g = \frac{1}{|g|} \sum_{k \in g} R_k, \quad (4)$$

and updates the policy by maximizing a clipped objective similar to PPO:

$$\mathcal{L}(\theta) = \mathbb{E}_i \left[\min \left(r_i(\theta) A_i, \text{clip}(r_i(\theta), 1 - \epsilon, 1 + \epsilon) A_i \right) \right], \quad (5)$$

where $r_i(\theta) = \frac{\pi_\theta(a_i | s_i)}{\pi_{\theta_{\text{old}}}(a_i | s_i)}$, a_i and s_i are the sampled action and state corresponding to rollout i , and ϵ is the PPO clipping parameter. By leveraging this group-relative advantage, GRPO stabilizes training across prompts, making the model robust to heterogeneous reward scales and noisy evaluations. Combined with our rubric-based reward and dynamic rollout selection strategy described below, we find GRPO can effectively guide the generative model toward images that are both human-aligned and high-quality.

3.4. Dynamic rollout sampling

As discussed above, the target policy model π_θ in GRPO explores the generation space by sampling multiple roll-

outs, each yielding a reward R_i used for advantage computation. In the original GRPO design, all N rollouts from a single prompt are grouped together for policy updates, *i.e.*, $|g| = N$. Subsequent works introduce over-sampling and filtering strategies to improve training efficiency. For instance, DAPO [55] adopts a *prompt-level* over-sampling approach: it generates N rollouts per prompt and discards prompts whose rollouts all have accuracy 1 or 0, thereby retaining only moderately difficult prompts for policy optimization. Formally, DAPO selectively sample prompts used in training while still using all rollouts from each retained prompt for RL updates.

In this paper, we propose a new *rollout-level* dynamic sampling mechanism, where selection occurs within the rollouts of a single prompt rather than filtering entire prompts. Specifically, given a text prompt, instead of sampling only N rollouts, we oversample N' rollouts ($N' > N$) and selectively use a subset of N representative rollouts for policy updates. To balance quality and diversity, we adopt a hybrid selection strategy: we take the top- K high-reward rollouts and randomly sample the remaining $N - K$ rollouts from the others to encourage diversity. Formally, the rollout group g is constructed as

$$g = \{\tau_{(1)}, \dots, \tau_{(K)}\} \cup \text{RS}(\{\tau_{(K+1)}, \dots, \tau_{(N')}\}, N - K),$$

where RS denotes random sampling. Empirically, we observe this hybrid design achieves a better balance between stability and diversity, achieving better model quality. As a result, the loss in Eq. 5 is computed over a more representative and informative subset of rollouts, leading to more consistent and efficient learning compared to both the original GRPO and the prompt-level filtering scheme in DAPO.

4. Experiments

4.1. Implementation details

Following SimpleAR [43], we select 11,000 images from JourneyDB [38] and Synthetic dataset-1M [12] and recaption the images using GPT-o4-mini to generate different prompt length per image and randomly pick up during training. For the network architecture, we use two LLM, *i.e.*, Phi3-3.8B [1] and Qwen2.5-0.5B [40] that have been SFT trained as the backbone, and use LlamaGen’s VQ decoder [39] and Cosmos-Tokenizer [2] as the visual decoder respectively. RL training is performed with TRL framework [42] at a learning rate of 1e-5 with a 0.1 warm-up ratio. The datasets are trained with a batch size of 28 for 3 epochs by default. The resolutions of output images in two backbones are 512 and 1024, respectively. For dynamic rollout sampling, we select 4 candidates from 16 rollouts per prompt. During inference, we leverage the classifier-free guidance (CFG) [20] to guide image synthesis based on the

Table 1. Evaluation of text-to-image generation trained on Phi3 (3.8B) and Qwen2.5 (0.5B) as AR backbone on the GenEval.

Backbone	Method	Single Object	Two Object	Counting	Colors	Position	Color Attribute	Overall
Phi3-3.8B	SFT model	0.9938	0.8939	0.4562	0.9255	0.72	0.585	0.7624
	CLIPScore [30]	0.9938	0.9242	0.525	0.9362	0.7725	0.7	0.8086
	HPSv2 [51]	0.9906	0.8813	0.5125	0.9441	0.7675	0.7205	0.8035
	Unified Reward [46]	0.9969	0.9318	0.4156	0.9388	0.815	0.7	0.7997
	LLaVA-Reward-Phi [58]	0.9844	0.8864	0.4719	0.9176	0.725	0.5975	0.7638
	AR-GRPO [56]	0.9938	0.8712	0.5406	0.9574	0.8075	0.63	0.8001
	X-Omni [14]	0.9969	0.9192	0.4719	0.9548	0.8175	0.6875	0.8080
	RubricRL	1.0	0.9343	0.6125	0.9415	0.8275	0.765	0.8468
Qwen2.5-0.5B	SFT model	0.9625	0.5303	0.25	0.7606	0.3575	0.2825	0.5239
	CLIPScore [30]	0.9656	0.6162	0.275	0.8404	0.3825	0.325	0.5674
	HPSv2 [51]	0.975	0.6465	0.2438	0.8005	0.3875	0.2825	0.5560
	Unified Reward [46]	0.9625	0.6288	0.2656	0.8191	0.4050	0.3550	0.5727
	LLaVA-Reward-Phi [58]	0.9625	0.5303	0.25	0.7606	0.3575	0.2825	0.5239
	AR-GRPO [56]	0.9656	0.5682	0.2969	0.8378	0.3825	0.3050	0.5593
	X-Omni [14]	0.9812	0.5960	0.2219	0.8085	0.4125	0.32	0.5567
	RubricRL	0.9844	0.6616	0.2469	0.8378	0.4825	0.3950	0.6014

Table 2. Evaluation of text-to-image generation trained on Phi3 (3.8B) and Qwen2.5 (0.5B) as AR backbone on the DPG-Bench.

Backbone	Method	Global	Entity	Attribute	Relation	Other	Overall
Phi3-3.8B	SFT model	84.80	87.90	88.18	93.30	82.0	81.25
	CLIPScore [30]	81.76	89.95	89.42	93.5	86.0	84.15
	HPSv2 [51]	82.98	90.71	89.94	93.19	87.6	84.85
	Unified Reward [46]	82.37	89.94	89.50	93.93	85.2	84.06
	LLaVA-Reward-Phi [58]	82.98	88.06	87.83	92.50	79.2	81.51
	AR-GRPO [56]	82.37	89.05	90.0	93.08	88.0	83.81
	X-Omni [14]	84.19	89.66	89.12	93.69	86.0	84.05
	RubricRL	83.28	91.88	90.07	94.73	85.2	86.07
Qwen2.5-0.5B	SFT model	84.78	84.74	86.41	87.34	84.27	78.02
	CLIPScore [30]	80.55	87.22	86.19	91.33	67.6	79.78
	HPSv2 [51]	78.42	87.29	85.04	91.45	68.8	80.23
	Unified Reward [46]	79.03	87.09	85.24	90.68	69.20	79.69
	LLaVA-Reward-Phi [58]	84.78	84.74	86.41	87.34	84.27	78.02
	AR-GRPO [56]	80.24	86.75	85.95	92.02	69.35	79.74
	X-Omni [14]	79.33	87.03	85.34	91.72	72.40	79.92
	RubricRL	79.33	88.48	86.55	91.37	68.0	81.43

conditional and unconditional logits. All experiments are conducted on 8 NVIDIA A100 GPUs.

4.2. Comparing with state-of-the-arts

We compare RubricRL with multiple reward models across aforementioned two text-to-image SFT models on DPG-Bench [22] and GenEval [47]. The compared reward methods can be grouped according to their reward design: 1) a single specialized reward model, including CLIPScore [30], HPSv2 [51], Unified Reward [46], and LLaVA-Reward-Phi [58]; and 2) composite reward metrics with fixed weights, such as AR-GRPO [56] and X-Omni [14]. For fair comparison, we obtain the baseline numbers by implementing their methods and use the same RL framework (GRPO) and settings, while the only difference is the design of reward functions. For better understanding gains brought by RL, we also report the performance of the initial SFT model, on top of which each RL reward is inde-

pendently applied. Quantitative results using both Phi3 and Qwen2.5 backbones are reported in Table 1 and Table 2. For GenEval, prompt rewriting is applied following [10] to ensure evaluation consistency. From the results, all RL post-trained methods consistently outperform the SFT baseline, confirming the benefit of reinforcement learning in enhancing image generation quality. And RubricRL achieves the best performance, surpassing X-Omni by approximately 4% on GenEval on both LLM backbones, highlighting the effectiveness and generalization of our rubric-based reward.

4.3. Ablation study

In this section, we conduct multiple ablation analysis. By default, all experiments are based on Phi3 and evaluated on the GenEval benchmark .

Strategies for dynamic rollout sampling. To investigate the impact of different selection strategies used by dynamic rollout sampling, we compare four methods, *i.e.*, RubricRL

Table 3. Comparison of dynamic rollout-sampling strategies used in GRPO.

Method	Single	Two	Count	Colors	Position	Color	Attr.	Overall
Vanilla	0.9906	0.9217	0.6031	0.9441	0.7975	0.7525		0.8349
FFKC-1D	1.0	0.9268	0.5656	0.9441	0.825	0.75		0.8353
DAPO	0.9969	0.9293	0.6125	0.9362	0.7975	0.7275		0.8333
Hybrid	1.0	0.9343	0.6125	0.9415	0.8275	0.765		0.8468

Table 4. Comparison of advantage computation in GRPO, with performance measured on GenEval.

Method	Single	Two	Count	Colors	Position	Color	Attr.	Overall
Global Norm	0.9938	0.9268	0.6781	0.9362	0.785	0.6825		0.8337
Local Norm	1.0	0.9343	0.6125	0.9415	0.8275	0.765		0.8468

without dynamic rollout sampling (Vanilla), FFKC-1D [16], DAPO [55], and our proposed hybrid strategy, and report the results in Table 3. Specifically, FFKC-1D also over-samples more rollouts and then keeps a diverse subset by first selecting a medoid (the rollout with reward closest to the median) and then greedily adding samples that maximize reward distance from already chosen ones. Compared to our hybrid strategy, FFKC-1D focuses too much on the diversity and ignore the importance of high quality rollouts. As shown in Table 3, our hybrid sampling strategy consistently achieves the best performance, surpassing both FFKC-1D and DAPO as well as the Vanilla baseline that directly uses four rollouts without any dynamics. Interestingly, FFKC-1D and DAPO do not outperform the vanilla baseline, suggesting that their dynamic prompt sampling and pure rollout diversity-driven sampling strategies fail to provide additional informative signals for RL. In contrast, our hybrid strategy effectively balances exploitation of high-reward rollouts and exploration of diverse candidates, enabling the policy model to leverage both higher-quality and diverse samples, resulting in more effective RL signal.

Normalization scope for advantages. In Eq. 4, the advantage used in GRPO is computed by normalizing rewards—using the mean and standard deviation—within a group of rollouts. Under our dynamic sampling strategy, only N rollouts are retained out of N' candidates. This raises an important design choice: should the normalization statistics (mean and standard deviation) be computed using all N' rollouts or only the retained N ? We denote these two variants as “Global Norm” and “Local Norm”, respectively. In Table 4, it reflects that “Local Norm” yields better performance. This is because normalizing within the retained subset better reflects the actual reward distribution that guides learning, preventing high-variance or low-quality rollouts from distorting the gradient direction.

RubricRL v.s. SFT with Best-of-N sampling. We further compare the proposed RubricRL with the SFT



Figure 4. Failure cases of GPT-o4-mini when grading counting on GenEval. The model misjudges instance counts under ambiguity.

Table 5. Comparison on GenEval of Best-of-N ($N = 8$) and our RL training for Phi3-3.8B (P-*) and Qwen2.5-0.5B (Q-*).

Method	Single	Two	Count	Colors	Position	Color	Attr.	Overall
P-SFT model	0.9938	0.8939	0.4562	0.9255	0.7200	0.5850		0.7624
P-Best-of-N	0.9812	0.9091	0.6000	0.9309	0.7450	0.5900		0.7927
P-RubricRL	1.0	0.9343	0.6125	0.9415	0.8275	0.765		0.8468
Q-SFT model	0.9625	0.5303	0.2500	0.7314	0.3575	0.2825		0.5239
Q-Best-of-N	0.9562	0.6566	0.3750	0.8138	0.4100	0.3600		0.5953
Q-RubricRL	0.9844	0.6616	0.2469	0.8378	0.4825	0.3950		0.6014

model equipped with a Best-of-N sampling strategy during inference ($N = 8$), which has been observed in prior work [14] to form a ‘upperbound’ for RL methods in language tasks. Specifically, for each prompt in GenEval, we first generate a rubric, then sample 8 rollouts from the SFT model. Each rollout is scored using the rubric-based reward, and the top 4 are selected for evaluation on GenEval. As shown in Table 5, although Best-of-N sampling significantly can achieve higher scores, RubricRL still achieves a notable improvement, exceeding it by over 5%. This result aligns with the observations in X-Omni [14], reconfirming that reinforcement learning provides a more effective optimization paradigm.

Failure case analysis. As the grader, although GPT-o4-mini is highly general and powerful in evaluating the quality of generated images, we observe that it can assign incorrect scores—*e.g.*, underestimating or overestimating object counts, particularly when the base model’s generation quality is poor. Figure 4 illustrates several typical failure cases in the counting subcategory of GenEval, such as redundant poles near traffic lights, intertwined bicycles, and overlapping zebras. These challenging scenarios often mislead GPT-o4-mini, resulting in inaccurate counts. However, when the base model generates higher-quality images, this issue is less pronounced. This explains why RubricRL’s performance on the “counting” subcategory in GenEval and the “Other” subcategory in DPG-Bench—both containing many counting cases—is worse than the baseline SFT model when using Qwen2.5-0.5B as the base model. In contrast, with Phi3-3.8B, this issue almost disappears, allowing RubricRL to substantially improve performance in

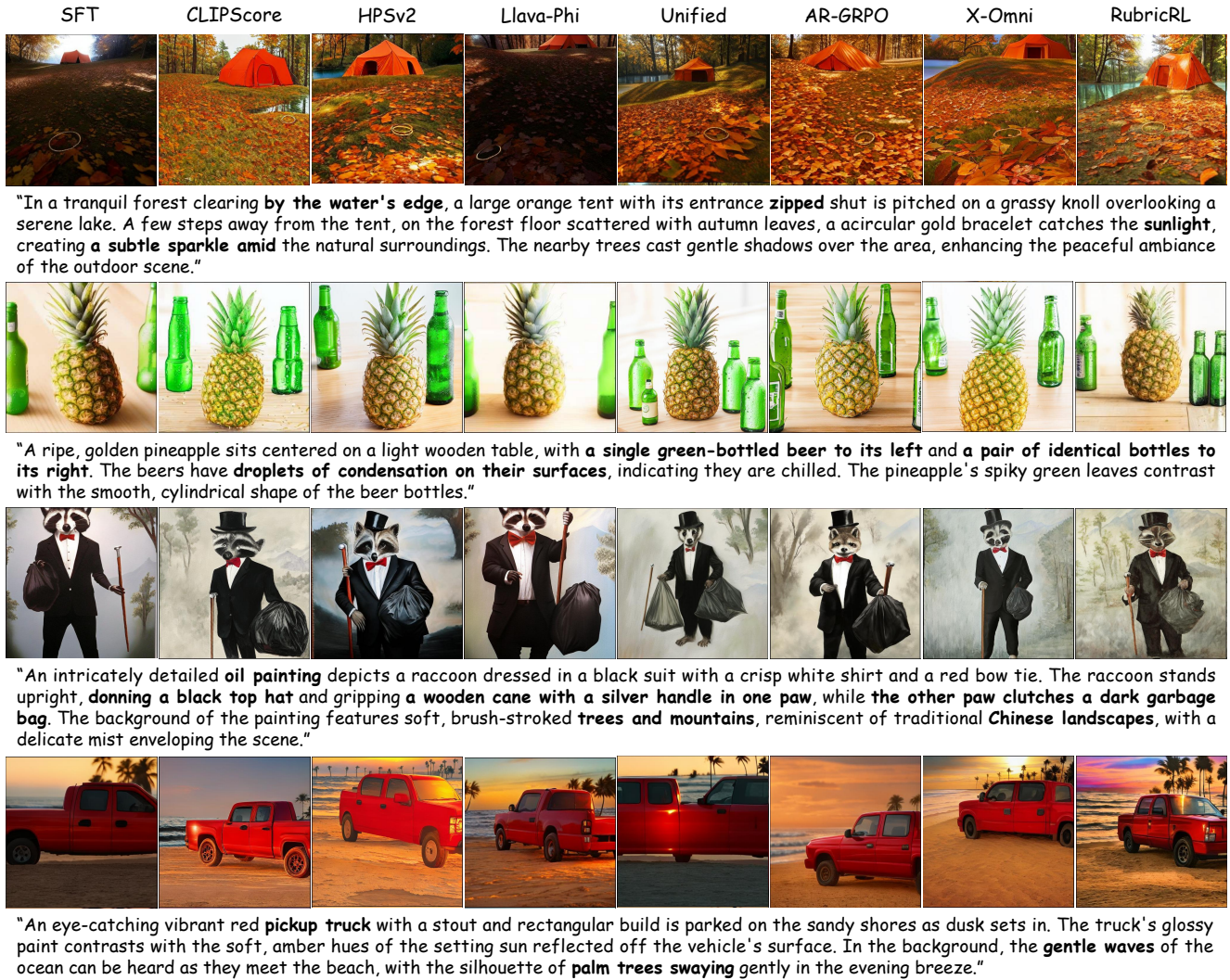


Figure 5. Qualitative comparison: we visualize RubricRL and baseline models using prompts from DPG. RubricRL shows superior image quality that is both aesthetically pleasing and better aligned with the prompt. The **bold text** highlights key elements that RubricRL successfully captures, while baseline models often fail to generate these details accurately.

counting-related categories.

4.4. Visual results

We further present comprehensive visual comparisons between RubricRL and other baseline approaches in Figure 5. As illustrated, models trained with RubricRL consistently produce images that are not only more aesthetically appealing but also demonstrate superior semantic alignment with the given input prompts. To aid interpretation, any misaligned or missing elements in the generated images are emphasized using bold text within the figure. For example, in the third row of Figure 5, the SFT model fails to render the black top hat entirely, while several RL-based methods exhibit partial misalignment. Specifically, LLaVA-Reward-Phi [58] and Unified Reward [46] generate outputs

where the black bag is not properly held in hand, and in some cases, depict two bags in both paws while omitting the wooden cane altogether. These qualitative observations underscore the effectiveness of RubricRL in enhancing the model’s capability to follow complex, fine-grained instructions and produce high-quality, prompt-consistent images.

5. Conclusion

In this paper, we introduce RubricRL, a rubric-based reward RL framework that provides prompt-adaptive, decomposable supervision for text-to-image generation. By explicitly creating configurable visual criteria (e.g., counting, attributes, OCR fidelity, realism) and scoring them independently, RubricRL produces interpretable and modu-

lar signals that integrate seamlessly with standard policy optimization in RL. Experimental results demonstrate that RubricRL outperforms existing RL-based approaches for enhancing text-to-image generation. We hope this work provides new insights into applying reinforcement learning to visual generation models.

References

- [1] Marah Abdin, Jyoti Aneja, Hany Awadalla, Ahmed Awadallah, Ammar Ahmad Awan, Nguyen Bach, Amit Bahree, Arash Bakhtiari, Jianmin Bao, Harkirat Behl, et al. Phi-3 technical report: A highly capable language model locally on your phone. *arXiv e-prints*, pages arXiv–2404, 2024. 5
- [2] Niket Agarwal, Arslan Ali, Maciej Bala, Yogesh Balaji, Erik Barker, Tiffany Cai, Prithvijit Chattopadhyay, Yongxin Chen, Yin Cui, Yifan Ding, et al. Cosmos world foundation model platform for physical ai. *arXiv preprint arXiv:2501.03575*, 2025. 5
- [3] Omri Avrahami, Dani Lischinski, and Ohad Fried. Blended diffusion for text-driven editing of natural images. In *Proceedings of the IEEE/CVF conference on computer vision and pattern recognition*, pages 18208–18218, 2022. 1
- [4] Shuai Bai, Keqin Chen, Xuejing Liu, Jialin Wang, Wenbin Ge, Sibao Song, Kai Dang, Peng Wang, Shijie Wang, Jun Tang, et al. Qwen2. 5-vl technical report. *arXiv preprint arXiv:2502.13923*, 2025. 3, 1
- [5] Huiwen Chang, Han Zhang, Jarred Barber, AJ Maschinot, Jose Lezama, Lu Jiang, Ming-Hsuan Yang, Kevin Murphy, William T Freeman, Michael Rubinstein, et al. Muse: Text-to-image generation via masked generative transformers. *arXiv preprint arXiv:2301.00704*, 2023. 3
- [6] Xi Chen, Nikhil Mishra, Mostafa Rohaninejad, and Pieter Abbeel. Pixelsnail: An improved autoregressive generative model. In *International conference on machine learning*, pages 864–872. PMLR, 2018. 1
- [7] Xiaokang Chen, Zhiyu Wu, Xingchao Liu, Zizheng Pan, Wen Liu, Zhenda Xie, Xingkai Yu, and Chong Ruan. Janus-pro: Unified multimodal understanding and generation with data and model scaling. *arXiv preprint arXiv:2501.17811*, 2025.
- [8] Jooyoung Choi, Sungwon Kim, Yonghyun Jeong, Youngjune Gwon, and Sungroh Yoon. Ilvr: Conditioning method for denoising diffusion probabilistic models. *arXiv preprint arXiv:2108.02938*, 2021. 1
- [9] Cheng Cui, Ting Sun, Manhui Lin, Tingquan Gao, Yubo Zhang, Jiakuan Liu, Xueqing Wang, Zelun Zhang, Changda Zhou, Hongen Liu, et al. Paddleocr 3.0 technical report. *arXiv preprint arXiv:2507.05595*, 2025. 2, 3
- [10] Chaorui Deng, Deyao Zhu, Kunchang Li, Chenhui Gou, Feng Li, Zeyu Wang, Shu Zhong, Weihao Yu, Xiaonan Nie, Ziang Song, et al. Emerging properties in unified multimodal pretraining. *arXiv preprint arXiv:2505.14683*, 2025. 6
- [11] Runpei Dong, Chunrui Han, Yuang Peng, Zekun Qi, Zheng Ge, Jinrong Yang, Liang Zhao, Jianjian Sun, Hongyu Zhou, Haoran Wei, et al. Dreamllm: Synergistic multimodal comprehension and creation. *arXiv preprint arXiv:2309.11499*, 2023. 3
- [12] Ben Egan, Alex Redden, XWAVE, and SilentAntagonist. Dalle3 1 Million+ High Quality Captions, 2024. 5
- [13] Patrick Esser, Sumith Kulal, Andreas Blattmann, Rahim Entezari, Jonas Müller, Harry Saini, Yam Levi, Dominik Lorenz, Axel Sauer, Frederic Boesel, et al. Scaling rectified flow transformers for high-resolution image synthesis. In *Forty-first international conference on machine learning*, 2024. 3
- [14] Zigang Geng, Yibing Wang, Yeyao Ma, Chen Li, Yongming Rao, Shuyang Gu, Zhao Zhong, Qinglin Lu, Han Hu, Xiaosong Zhang, et al. X-omni: Reinforcement learning makes discrete autoregressive image generative models great again. *arXiv preprint arXiv:2507.22058*, 2025. 2, 6, 7
- [15] Yuan Gong, Xionghui Wang, Jie Wu, Shiyin Wang, Yitong Wang, and Xinglong Wu. Onereward: Unified mask-guided image generation via multi-task human preference learning. *arXiv preprint arXiv:2508.21066*, 2025. 2
- [16] Teofilo F Gonzalez. Clustering to minimize the maximum intercluster distance. *Theoretical computer science*, 38:293–306, 1985. 7
- [17] Shuyang Gu, Dong Chen, Jianmin Bao, Fang Wen, Bo Zhang, Dongdong Chen, Lu Yuan, and Baining Guo. Vector quantized diffusion model for text-to-image synthesis. In *Proceedings of the IEEE/CVF conference on computer vision and pattern recognition*, pages 10696–10706, 2022. 3
- [18] Anisha Gunjal, Anthony Wang, Elaine Lau, Vaskar Nath, Yunzhong He, Bing Liu, and Sean Hendryx. Rubrics as rewards: Reinforcement learning beyond verifiable domains. *arXiv preprint arXiv:2507.17746*, 2025. 3
- [19] Daya Guo, Dejian Yang, Haowei Zhang, Junxiao Song, Ruoyu Zhang, Runxin Xu, Qihao Zhu, Shirong Ma, Peiyi Wang, Xiao Bi, et al. Deepseek-r1: Incentivizing reasoning capability in llms via reinforcement learning. *arXiv preprint arXiv:2501.12948*, 2025. 2
- [20] Jonathan Ho and Tim Salimans. Classifier-free diffusion guidance. *arXiv preprint arXiv:2207.12598*, 2022. 5
- [21] Jonathan Ho, Ajay Jain, and Pieter Abbeel. Denoising diffusion probabilistic models. *Advances in neural information processing systems*, 33:6840–6851, 2020. 1
- [22] Xiwei Hu, Rui Wang, Yixiao Fang, Bin Fu, Pei Cheng, and Gang Yu. Ella: Equip diffusion models with llm for enhanced semantic alignment. *arXiv preprint arXiv:2403.05135*, 2024. 6
- [23] Zenan Huang, Yihong Zhuang, Guoshan Lu, Zeyu Qin, Haokai Xu, Tianyu Zhao, Ru Peng, Jiaqi Hu, Zhanming Shen, Xiaomeng Hu, et al. Reinforcement learning with rubric anchors. *arXiv preprint arXiv:2508.12790*, 2025. 3
- [24] Dongzhi Jiang, Ziyu Guo, Renrui Zhang, Zhuofan Zong, Hao Li, Le Zhuo, Shilin Yan, Pheng-Ann Heng, and Hongsheng Li. T2i-r1: Reinforcing image generation with collaborative semantic-level and token-level cot. *arXiv preprint arXiv:2505.00703*, 2025. 3
- [25] George Karypis, Eui-Hong Han, and Vipin Kumar. Chameleon: Hierarchical clustering using dynamic modeling. *computer*, 32(8):68–75, 1999. 3
- [26] Shufan Li, Konstantinos Kallidromitis, Akash Gokul, Zichun Liao, Yusuke Kato, Kazuki Kozuka, and Aditya Grover. Omniflow: Any-to-any generation with multi-modal rectified

- flows. In *Proceedings of the Computer Vision and Pattern Recognition Conference*, pages 13178–13188, 2025. 3
- [27] Jie Liu, Gongye Liu, Jiajun Liang, Yangguang Li, Jiaheng Liu, Xintao Wang, Pengfei Wan, Di Zhang, and Wanli Ouyang. Flow-grpo: Training flow matching models via online rl. *arXiv preprint arXiv:2505.05470*, 2025. 3
- [28] Alex Nichol, Prafulla Dhariwal, Aditya Ramesh, Pranav Shyam, Pamela Mishkin, Bob McGrew, Ilya Sutskever, and Mark Chen. Glide: Towards photorealistic image generation and editing with text-guided diffusion models. *arXiv preprint arXiv:2112.10741*, 2021. 3
- [29] Long Ouyang, Jeffrey Wu, Xu Jiang, Diogo Almeida, Carroll Wainwright, Pamela Mishkin, Chong Zhang, Sandhini Agarwal, Katarina Slama, Alex Ray, et al. Training language models to follow instructions with human feedback. *Advances in neural information processing systems*, 35:27730–27744, 2022. 1
- [30] Alec Radford, Jong Wook Kim, Chris Hallacy, Aditya Ramesh, Gabriel Goh, Sandhini Agarwal, Girish Sastry, Amanda Askell, Pamela Mishkin, Jack Clark, et al. Learning transferable visual models from natural language supervision. In *International conference on machine learning*, pages 8748–8763. Pmlr, 2021. 2, 3, 6
- [31] Aditya Ramesh, Mikhail Pavlov, Gabriel Goh, Scott Gray, Chelsea Voss, Alec Radford, Mark Chen, and Ilya Sutskever. Zero-shot text-to-image generation. In *International conference on machine learning*, pages 8821–8831. Pmlr, 2021. 1
- [32] Robin Rombach, Andreas Blattmann, Dominik Lorenz, Patrick Esser, and Björn Ommer. High-resolution image synthesis with latent diffusion models. In *Proceedings of the IEEE/CVF conference on computer vision and pattern recognition*, pages 10684–10695, 2022. 1, 3
- [33] John Schulman, Filip Wolski, Prafulla Dhariwal, Alec Radford, and Oleg Klimov. Proximal policy optimization algorithms. *arXiv preprint arXiv:1707.06347*, 2017. 2
- [34] Zhihong Shao, Peiyi Wang, Qihao Zhu, Runxin Xu, Junxiao Song, Xiao Bi, Haowei Zhang, Mingchuan Zhang, YK Li, Yang Wu, et al. Deepseekmath: Pushing the limits of mathematical reasoning in open language models. *arXiv preprint arXiv:2402.03300*, 2024. 1, 5
- [35] Jascha Sohl-Dickstein, Eric Weiss, Niru Maheswaranathan, and Surya Ganguli. Deep unsupervised learning using nonequilibrium thermodynamics. In *International conference on machine learning*, pages 2256–2265. pmlr, 2015. 1
- [36] Yang Song and Stefano Ermon. Generative modeling by estimating gradients of the data distribution. *Advances in neural information processing systems*, 32, 2019.
- [37] Yang Song, Jascha Sohl-Dickstein, Diederik P Kingma, Abhishek Kumar, Stefano Ermon, and Ben Poole. Score-based generative modeling through stochastic differential equations. *arXiv preprint arXiv:2011.13456*, 2020. 1
- [38] Keqiang Sun, Junting Pan, Yuying Ge, Hao Li, Haodong Duan, Xiaoshi Wu, Renrui Zhang, Aojun Zhou, Zipeng Qin, Yi Wang, et al. Journeymb: A benchmark for generative image understanding. *Advances in neural information processing systems*, 36:49659–49678, 2023. 5
- [39] Peize Sun, Yi Jiang, Shoufa Chen, Shilong Zhang, Bingyue Peng, Ping Luo, and Zehuan Yuan. Autoregressive model beats diffusion: Llama for scalable image generation. *arXiv preprint arXiv:2406.06525*, 2024. 1, 5
- [40] Qwen Team et al. Qwen2.5 technical report. *arXiv preprint arXiv:2407.10671*, 2(3), 2024. 5
- [41] Keyu Tian, Yi Jiang, Zehuan Yuan, Bingyue Peng, and Liwei Wang. Visual autoregressive modeling: Scalable image generation via next-scale prediction. *Advances in neural information processing systems*, 37:84839–84865, 2024. 1
- [42] Leandro von Werra, Younes Belkada, Lewis Tunstall, Edward Beeching, Tristan Thrush, Nathan Lambert, Shengyi Huang, Kashif Rasul, and Quentin Gallouédec. Trl: Transformer reinforcement learning. <https://github.com/huggingface/trl>, 2020. 5
- [43] Junke Wang, Zhi Tian, Xun Wang, Xinyu Zhang, Weilin Huang, Zuxuan Wu, and Yu-Gang Jiang. Simplear: Pushing the frontier of autoregressive visual generation through pre-training, sft, and rl. *arXiv preprint arXiv:2504.11455*, 2025. 3, 5
- [44] Xinlong Wang, Xiaosong Zhang, Zhengxiong Luo, Quan Sun, Yufeng Cui, Jinsheng Wang, Fan Zhang, Yueze Wang, Zhen Li, Qiyang Yu, et al. Emu3: Next-token prediction is all you need. *arXiv preprint arXiv:2409.18869*, 2024. 3
- [45] Yibin Wang, Zhimin Li, Yuhang Zang, Yujie Zhou, Jiazi Bu, Chunyu Wang, Qinglin Lu, Cheng Jin, and Jiaqi Wang. Pref-grpo: Pairwise preference reward-based grpo for stable text-to-image reinforcement learning. *arXiv preprint arXiv:2508.20751*, 2025. 2, 3
- [46] Yibin Wang, Yuhang Zang, Hao Li, Cheng Jin, and Jiaqi Wang. Unified reward model for multimodal understanding and generation. *arXiv preprint arXiv:2503.05236*, 2025. 3, 6, 8
- [47] Haoran Wei, Chenglong Liu, Jinyue Chen, Jia Wang, Lingyu Kong, Yanming Xu, Zheng Ge, Liang Zhao, Jianjian Sun, Yuang Peng, et al. General ocr theory: Towards ocr-2.0 via a unified end-to-end model. *arXiv preprint arXiv:2409.01704*, 2024. 3, 6
- [48] Tianyi Wei, Dongdong Chen, Yifan Zhou, and Xingang Pan. Enhancing mmdit-based text-to-image models for similar subject generation. *arXiv preprint arXiv:2411.18301*, 2024. 3
- [49] Chengyue Wu, Xiaokang Chen, Zhiyu Wu, Yiyang Ma, Xingchao Liu, Zizheng Pan, Wen Liu, Zhenda Xie, Xingkai Yu, Chong Ruan, et al. Janus: Decoupling visual encoding for unified multimodal understanding and generation. In *Proceedings of the Computer Vision and Pattern Recognition Conference*, pages 12966–12977, 2025. 3
- [50] Chenfei Wu, Jiahao Li, Jingren Zhou, Junyang Lin, Kaiyuan Gao, Kun Yan, Sheng-ming Yin, Shuai Bai, Xiao Xu, Yilei Chen, et al. Qwen-image technical report. *arXiv preprint arXiv:2508.02324*, 2025. 3
- [51] Xiaoshi Wu, Yiming Hao, Keqiang Sun, Yixiong Chen, Feng Zhu, Rui Zhao, and Hongsheng Li. Human preference score v2: A solid benchmark for evaluating human preferences of text-to-image synthesis. *arXiv preprint arXiv:2306.09341*, 2023. 2, 3, 6
- [52] Zeyue Xue, Jie Wu, Yu Gao, Fangyuan Kong, Lingting Zhu, Mengzhao Chen, Zhiheng Liu, Wei Liu, Qiushan Guo,

- Weilin Huang, et al. Dancegrpo: Unleashing grpo on visual generation. *arXiv preprint arXiv:2505.07818*, 2025. 3
- [53] Sidi Yang, Tianhe Wu, Shuwei Shi, Shanshan Lao, Yuan Gong, Mingdeng Cao, Jiahao Wang, and Yujiu Yang. Maniqa: Multi-dimension attention network for no-reference image quality assessment. In *Proceedings of the IEEE/CVF conference on computer vision and pattern recognition*, pages 1191–1200, 2022. 3
- [54] Jiahui Yu, Yuanzhong Xu, Jing Yu Koh, Thang Luong, Gunjan Baid, Zirui Wang, Vijay Vasudevan, Alexander Ku, Yinfei Yang, Burcu Karagol Ayan, et al. Scaling autoregressive models for content-rich text-to-image generation. *arXiv preprint arXiv:2206.10789*, 2(3):5, 2022. 3
- [55] Qiyang Yu, Zheng Zhang, Ruofei Zhu, Yufeng Yuan, Xiaochen Zuo, Yu Yue, Weinan Dai, Tiantian Fan, Gao-hong Liu, Lingjun Liu, et al. Dapo: An open-source llm reinforcement learning system at scale. *arXiv preprint arXiv:2503.14476*, 2025. 1, 5, 7
- [56] Shihao Yuan, Yahui Liu, Yang Yue, Jingyuan Zhang, Wangmeng Zuo, Qi Wang, Fuzheng Zhang, and Guorui Zhou. Ar-grpo: Training autoregressive image generation models via reinforcement learning. *arXiv preprint arXiv:2508.06924*, 2025. 2, 6
- [57] Chunting Zhou, Lili Yu, Arun Babu, Kushal Tirumala, Michihiro Yasunaga, Leonid Shamis, Jacob Kahn, Xuezhe Ma, Luke Zettlemoyer, and Omer Levy. Transfusion: Predict the next token and diffuse images with one multi-modal model. *arXiv preprint arXiv:2408.11039*, 2024. 3
- [58] Shijie Zhou, Ruiyi Zhang, Huaisheng Zhu, Branislav Kveton, Yufan Zhou, Jiuxiang Gu, Jian Chen, and Changyou Chen. Multimodal llms as customized reward models for text-to-image generation. In *Proceedings of the IEEE/CVF International Conference on Computer Vision*, pages 19638–19648, 2025. 2, 3, 6, 8

RubricRL: Simple Generalizable Rewards for Text-to-Image Generation

Supplementary Material

Table 6. Comparison of different grader models, with performance measured on GenEval.

Grader	Single	Two	Count	Colors	Position	Color Attr.	Overall
Qwen2.5-3B	0.9938	0.9141	0.4562	0.9441	0.7875	0.6475	0.7906
Qwen2.5-7B	0.9969	0.899	0.5031	0.9415	0.7425	0.6925	0.7959
Qwen2.5-32B	0.9969	0.9268	0.5688	0.9149	0.7725	0.6925	0.8121
Ours (o4-mini)	1.0	0.9343	0.6125	0.9415	0.8275	0.765	0.8468

6. More ablations

6.1. Analysis of using different models as the grader.

Our method, *i.e.*, RubricRL benefits from a high-quality grader (GPT-o4-mini) in RL: only when per-criterion judgments (*e.g.*, counting, spatial relations, color) are accurate does the reward become informative enough to drive useful policy updates. A weak or noisy grader produces misaligned signals that the policy can overfit or exploit, thereby hurting stability and sample efficiency. By contrast, a reliable grader yields low-noise, goal-aligned rewards that assign credit to the right behaviours and penalize specific errors, making RubricRL effective.

To quantify this effect, we use different vision language models as the grader in RubricRL and report the results in Table 6. We choose the Qwen2.5-VL [4] family with varying model sizes (3B, 7B, and 32B) to evaluate each rollout during training. We observe that the 32B grader clearly outperforms both the 3B and 7B variants, confirming that a stronger vision–language model provides more informative and reliable rewards overall. The 7B model shows a slight improvement over the 3B model, consistent with its higher capacity, while the 3B grader still offers useful signals on certain criteria (*e.g.*, color and position). Nevertheless, both Qwen2.5-VL graders remain noticeably weaker than the 32B grader while all Qwen2.5-VL graders still lag behind the o4-mini grader with a clear gap, which we attribute to o4-mini’s stronger instruction following, better multi-step reasoning, and tighter alignment with our rubric design, resulting in sharper, lower-noise per-criterion rewards and ultimately better downstream generation quality.

6.2. Analysis of the number of rollouts before and after dynamic sampling.

We investigate how the oversampling budget and the post selection budget, *i.e.*, how many rollouts we generate in the dynamic sampling versus how many we keep for reward computation, affect the model’s performance. For each prompt, we first generate N' candidate rollouts ($N' > N$) and then select N of them using our Hybrid dynamic sam-

Table 7. Comparison of different numbers N' of oversampled rollouts and different numbers N selected). In the main paper, the setting is $N' = 16$, $N = 4$.

Number of N'	Single	Two	Count	Colors	Position	Color Attr.	Overall
$N = 4$							
$N' = 8$	0.9906	0.9293	0.60	0.9362	0.795	0.72	0.8285
$N' = 16$	1.0	0.9343	0.6125	0.9415	0.8275	0.765	0.8468
$N' = 32$	0.9906	0.9318	0.5875	0.9388	0.795	0.755	0.8331
$N' = 64$	0.9938	0.9268	0.5844	0.9388	0.795	0.765	0.8340
$N = 8$							
$N' = 16$	0.9969	0.9192	0.5781	0.9362	0.8025	0.7575	0.8317
$N' = 32$	0.9906	0.9141	0.6094	0.9468	0.8225	0.7775	0.8435
$N' = 64$	0.9875	0.9343	0.6094	0.9388	0.815	0.735	0.8367

pling strategy; the selected N samples are used to compute the GRPO loss. All other hyperparameters remain fixed across settings.

As shown in Table 7, increasing the oversampling budget (*e.g.*, $N' \in \{8, 16, 32, 64\}$) with fixed $N = 4$) initially improves performance by providing a larger candidate pool from which the Hybrid selector can identify high-reward and diverse rollouts. However, the gains soon saturate because larger N' also introduces higher reward variance, making advantage estimates noisier and hindering stable optimization. A similar phenomenon appears when increasing the selection budget from $N = 4$ to $N = 8$: although more selected rollouts increase exploitation, incorporating too many rollouts increases the likelihood of including low-quality generations, amplifying variance in the group-normalized advantage and diluting the learning signal. Notably, configurations with a $4\times$ oversampling ratio achieve comparable overall performance, indicating that maintaining this level of oversampling is sufficient for obtaining high-quality candidates. Overall, both oversampling and selection are beneficial only up to a point—beyond that, the added diversity is outweighed by increased noise, revealing an inherent trade-off between exploration and optimization stability in GRPO-style training.

7. Visualization

In this section, we present additional generations from our RubricRL. As shown in Figure 6, our RubricRL produces high-fidelity images, and significantly improves the model’s ability to follow complex prompts. Additionally, we visualize the detailed key-criterion rubrics for each prompt, along with the correctness or incorrectness of each rollout under each criterion, as shown in Figure 7.



In this whimsical digital illustration, a plump guinea pig is rendered in a vibrant palette of orange, cream, navy blue, and vivid purple. Its fur is stylized with fine, dynamic strokes, while a tuft of lime green hair sweeps back over its head, adding playful contrast. The rodent's rosy pink paws and ears peek out from the dense coat, and its shiny black eye gleams with life. Set against a muted olive-green background, the guinea pig's rounded form and richly saturated colors create a charming blend of realism and fantasy, evoking both warmth and imaginative flair.



A tiny red squirrel nestles into a soft mound of fresh snow atop a moss-covered branch, its bushy tail curled protectively around its body. Fine snowflakes cling to the animal's warm fur and the overhanging pine needles, while clusters of frosted leaves and bright red berries add subtle bursts of color to the muted winter palette. The squirrel's delicate paws are tucked close to its chest, and its eyes are gently closed as if in a peaceful slumber. Soft light filters through the bare branches above, casting a faint glow across the scene and highlighting the intricate textures of fur, bark, and frost in this serene woodland tableau.



Arranged in a perfect three-by-three grid against a smooth, muted tan surface, these doughnuts each display unique artistic flair through bright pastel glazes and playful toppings. The top row features a yellow-glazed doughnut with pastel drizzles, a golden doughnut adorned with frosting dollops and multicolored sprinkles, and a teal-glazed ring speckled with fine rainbow sprinkles. The middle row presents a smooth turquoise square-edged ring, a deeper teal doughnut with glossy drizzle lines, and a scalloped-edge doughnut topped with almond pieces and candy-coated seeds. The bottom row offers a dark charcoal doughnut with cream-colored stripes, a dripping aqua-glazed doughnut blending round and square contours, and a pink-glazed classic ring covered in rainbow sprinkles, creating a visually harmonious, mouthwatering display.



An inviting black ceramic bowl with subtle golden speckles and a pale green rim holds a generous serving of thick, tomato-based bean stew. Plump yellow and beige beans are nestled in a rich mahogany sauce flecked with tiny ribbons of red pepper and minced onion. The bowl rests on a sunlit mustard-yellow saucer, creating a warm contrast against the cool teal backdrop. The stew's glossy surface catches highlights that accentuate its hearty texture, while the varied sizes and shapes of the beans suggest a comforting, homemade quality. Overall, the composition emphasizes the rustic simplicity and satisfying warmth of a classic bean stew ready to be enjoyed.



Bathed in the warm hues of a surreal sunset, this sleek Nike soccer cleat stands out with its streamlined silhouette, textured upper, and signature swoosh logo glowing softly against a twilight sky. The vibrant orange and purple tones blend seamlessly with the illuminated studs and grass beneath, while a soft, ethereal light trace curves over the shoe, suggesting movement and energy. Every detail—from the fine ridges on the surface to the subtle transition of colors—evokes a sense of high performance and cutting-edge design. This image highlights the fusion of technology and artistry in modern sportswear, capturing the spirit of competition and innovation.



In this black-and-white portrait, a sophisticated young woman gazes directly at the viewer with piercing eyes and perfectly sculpted eyebrows. Her skin appears porcelain smooth, subtly illuminated by soft, diffuse lighting that accentuates the contours of her high cheekbones and the gentle curve of her jawline. A wide-brimmed, woven white hat frames her face, casting a delicate shadow across her forehead, while her short, wavy hair peeks out in artful tousles. She wears a crisp white blouse adorned with a lace-trimmed scarf tied at her shoulder, adding a touch of vintage elegance. The minimalist background ensures that every nuance of her expression and attire remains in sharp relief, creating a timeless, refined aesthetic.



A rugged man stares directly at the viewer, his striking blue eyes framed by a tousled fringe and a medium-length beard flecked with gray. He wears a dark, textured hood over a patterned scarf, layers of coarse fabric that suggest a harsh environment or long journey. A smudge of black paint covers one cheek, blending into the shadowed contours of his face and hinting at camouflage or ritual markings. The low, dramatic lighting emphasizes the depth of his gaze and the rough textures of his clothing, creating an atmosphere of quiet determination and resilience.



In this captivating image, a youthful face emerges from a tapestry of vibrant botanical elements, her brilliant cerulean eyes brimming with quiet intensity. Soft freckles dust her nose and cheeks, where delicate purple petals cluster like living confetti, blurring the line between human and floral. Lush green leaves frame her forehead, intertwining with violet blossoms that seem to grow organically from her skin. The subtle interplay of light reveals the smooth, porcelain-like texture of her complexion, while shadows deepen the contours of her lips and jawline. The overall composition evokes a sense of ethereal beauty and fragile harmony between nature and the human form.



This intricate miniature tree sculpture features a dark, twisted trunk and coiling roots that rise from a sleek black ceramic pot. Tiny glass or gemstone accents in vivid teal are nestled among the branches, catching light and adding a mystical quality. Delicate leaves in shades of fresh green, soft blue, and warm orange form a lush canopy, creating a stunning contrast against the dark wood. The bonsai-inspired form combines natural and fantastical elements, evoking both ancient artistry and modern design. Subtle variations in texture and color throughout the branches draw the eye, making this piece a captivating blend of sculpture and living-inspired art.



A charming log cabin emerges from a lush forest clearing at the base of a majestic, snow-dusted mountain. Framed by tall, slender pines, the cabin's warm wooden walls and green-painted door and window shutters stand in stark contrast to the cool emerald hues of surrounding foliage. A gentle slope leads down to a crystal-clear lake, its glassy surface mirroring the cabin, scattered boulders, and the dense tree line beyond. Soft golden light filters through the evergreens, casting dappled shadows across the grassy shore, while faint sparks of embers or distant firelight glow within the woods. The scene evokes serene solitude and an intimate connection with nature, promising peaceful retreats and quiet moments by the water's edge.



In this intimate interior scene, a vintage wooden frame mounted on a softly painted pastel pink wall presents a two-panel impressionist landscape. The upper panel reveals a sunlit sky dotted with wispy clouds drifting above a canopy of fiery orange blooms, while the lower panel immerses the viewer in a lush garden scene, brimming with vibrant petals and verdant foliage. To the left, a gently draped textured pink curtain adds depth and warmth, its subtle folds catching ambient light. The juxtaposition of the blooming floral artwork against the monochromatic wall and curtain creates a harmonious composition, an inviting contemplation of color, texture, and the serene beauty of nature rendered in soft, painterly strokes.



Soft pastel light bathes a tranquil mountain basin in rosy hues as jagged, ivory peaks rise in the distance above a placid river. Towering green cliffs on either side slope gently toward the water's edge, where clumps of grass and clusters of vibrant pink blossoms peek from mossy banks. A lone, gracefully curved tree stands sentinel on a rocky outcrop, its russet foliage contrasting against the peach sky. Wisps of cloud drift above the horizon and a flock of tiny birds flutters near the summit, lending a sense of quiet wonder to this dreamlike landscape. The entire scene exudes an otherworldly serenity, inviting contemplation and awe.

Figure 6. More qualitative results showcasing diverse generations produced by our RubricRL model. The samples exhibit strong prompt following, stylistic versatility, and detailed visual quality.



"Rendered with precise, soft graphite strokes, this monochrome portrait captures an elderly woman in a three-quarter profile. Her silvery hair, styled in soft waves, peeks out beneath a brimmed hat adorned with a delicate ribbon. Greatly detailed lines trace the gentle contours of her forehead, the subtle creases around her watchful eyes, and the graceful slope of her jawline. A pair of dangling pearl earrings catches the faintest hint of light, complementing the ornate, leaf-like pendant that rests lightly against her collarbone. Her thoughtful expression, poised and dignified, evokes a lifetime of insight and quiet resilience, while the tonal shading lends both depth and warmth to the composition."

- "Style and Prompt Consistency": "Verify that the image uses soft graphite strokes in a monochrome portrait and maintains the three-quarter profile angle as described." ✓
- "Aesthetic Quality": "Verify that the final image is high quality, with clear lines, balanced contrast, smooth shading, and no rendering artifacts." ✓
- "Monochrome Compliance": "Ensure the image uses only shades of gray without any unintended colors." ✓
- "Style and Prompt Consistency": "Verify that the texture and line work convincingly replicate soft graphite pencil strokes." ✓
- "Object Count Consistency": "Verify that exactly one elderly woman is depicted in the portrait." ✓
- "Object Placement and Spatial Reasoning": "Ensure the subject's face is oriented in a three-quarter profile as specified." ✓
- "Attribute Accuracy": "Confirm silvery hair styled in soft waves and a brimmed hat with a delicate ribbon match the prompt." ✓
- "Attribute Accuracy": "Ensure detailed lines trace gentle forehead contours, subtle eye creases, jawline slope, and a thoughtful expression." ✓
- "Attribute Accuracy": "Verify that the dangling pearl earrings and leaf-like pendant are clearly rendered and capture subtle highlights." ✓
- "Scene Coherence": "Verify that tonal shading lends depth and warmth and that the light source is consistent across the portrait." ✓



"In this stylized retro landscape, a vast alpine lake stretches across the foreground, its glassy teal surface gently reflecting the rugged slopes of sun-drenched mountains. Tall, dark pine trees crowd the shoreline, their silhouettes contrasting with the warm ochre and sienna tones of the rocky ridges. Jagged peaks reach toward a sky patterned with soft, layered clouds in muted creams and greens, creating a serene yet dramatic vista. The composition evokes a vintage travel poster aesthetic, emphasizing bold shapes and harmonious color blocks. It captures the timeless beauty of mountainous wilderness, inviting viewers to imagine crisp air, silent waters, and the majesty of nature's grandeur."

- "Style and Prompt Consistency": "Ensure the image evokes a stylized retro vintage travel poster aesthetic with bold shapes and color blocks." ✓
- "Attribute Accuracy": "Verify that the lake's surface is rendered in a glassy teal hue with clear reflections." ✓
- "Attribute Accuracy": "Ensure mountain slopes display warm ochre and sienna tones as described." ✓
- "Attribute Accuracy": "Check that the sky's layered clouds are in muted creams and greens." ✓
- "Attribute Accuracy": "Confirm tall pine trees appear as dark silhouettes with sharp outlines." ✓
- "Object Placement and Spatial Reasoning": "Verify the lake is in the foreground, trees along the shoreline, and mountains reflected appropriately." ✓
- "Scene Coherence": "Check that lighting, perspective, and environmental details form a cohesive alpine wilderness scene." ✓
- "Aesthetic Quality": "Assess that the image is high quality with crisp lines, harmonious colors, and no distracting artifacts." ✓
- "Scene Coherence": "Evaluate the harmony between teal, ochre, sienna, and muted neutrals across the composition." ✓
- "Scene Coherence": "Verify that shapes and color blocks are balanced and harmonious across the composition." ✓



"In the heart of a shadowy 1940s-inspired bar, a poised woman with softly curled hair and an elegant satin dress leans against the polished wooden counter, a half-full wine glass delicately held in her slender fingers. Her thoughtful gaze drifts toward the glowing neon sign that reads 'COELE', casting a faint halo over the bottles lined up behind her. The low-hung lamps create pools of warm light, accentuating the shimmer of her chandelier earrings and the subtle sparkle of her beaded necklace. An air of quiet contemplation wraps around her lacquered lips and arched brows, hinting at untold stories beneath her composed facade. The entire scene, rendered in timeless black and white, evokes the moody elegance of film noir, where every shadow whispers intrigue and every sip could mark the beginning of a secret moment."

- "OCR Alignment": "Ensure the glowing neon sign clearly reads 'COELE' with correct letter shapes and placement." ✓
- "Action Accuracy": "Verify the woman is leaning against the counter, holding a half-full wine glass in her slender fingers, and gazing thoughtfully at the neon sign." ✓
- "Object Count Consistency": "Verify that exactly one woman and one neon sign are present as specified in the prompt." ✓
- "Object Count Consistency": "Confirm that exactly one half-full wine glass is present." ✓
- "Object Placement and Spatial Reasoning": "Ensure the woman is positioned at the bar counter with bottles behind her and the neon sign casting light above." ✓
- "Attribute Accuracy": "Verify that the woman has softly curled hair, an elegant satin dress, chandelier earrings, a beaded necklace, lacquered lips, and arched brows as described." ✓
- "Scene Coherence": "Verify that the lighting creates pools of warm light and high-contrast shadows, evoking the moody elegance of film noir." ✓
- "Style and Prompt Consistency": "Ensure the image is rendered in black and white with a film noir aesthetic and moody high-contrast lighting." ✓
- "Aesthetic Quality": "Assess overall image quality for sharpness, realistic lighting pools, and absence of artifacts to evoke a 1940s ambiance." ✓
- "Scene Coherence": "Verify that the bar environment—including wooden counter, low-hung lamps, and lined bottles—is cohesive and contextually appropriate." ✓



"A tall, slender model wears a striking cream-colored ensemble that blends minimalist tailoring with high-tech details. The oversized jacket features a structured high collar, broad sleeves, and large front pockets, while translucent vinyl-like panels at the shoulders reveal a hidden amber layer beneath. Matching knee-length shorts continue the streamlined silhouette, accented by subtle piping that echoes the jacket's edges. The model's sharp, close-cropped haircut and neutral makeup underscore the collection's futuristic aesthetic. Surrounding the figure are large, fluffy blossoms in muted peach tones, their organic shapes contrasting gently with the outfit's clean lines and synthetic materials. The overall scene conveys an intriguing dialogue between nature and innovation, presenting a vision of modern fashion that is at once bold, refined, and forward-looking."

- "Style and Prompt Consistency": "Verify that the image reflects a high-fashion editorial style with a futuristic aesthetic as described." ✓
- "Aesthetic Quality": "Verify that the image is high resolution with realistic lighting, sharp focus, and no rendering artifacts." ✓
- "Attribute Accuracy": "Verify that the ensemble is cream-colored with minimalist tailoring and high-tech details." ✓
- "Attribute Accuracy": "Verify that the oversized jacket has a structured high collar, broad sleeves, and large front pockets as described." ✓
- "Attribute Accuracy": "Verify translucent vinyl-like panels are present at the shoulders and reveal a discernible amber layer beneath." ✓
- "Attribute Accuracy": "Verify that subtle piping echoes the edges of the jacket and shorts." ✓
- "Attribute Accuracy": "Verify that the model wears streamlined, knee-length shorts matching the jacket." ✗
- "Attribute Accuracy": "Verify that the model has a sharp, close-cropped haircut and neutral makeup." ✓
- "Attribute Accuracy": "Verify that the blossoms are large, fluffy, and rendered in muted peach tones." ✓
- "Scene Coherence": "Verify that the overall composition and lighting convey a balanced dialogue between nature and innovation." ✓



"Two fledgling owls, tiny and round, are nestled side by side within a bed of dried grasses and twigs. Their downy plumage, mottled with white speckles atop a warm brown base, catches the sunlight filtering through tall meadow stalks. Each owl's large, luminous eyes, rimmed in gold and encircled by soft facial discs, convey a look of curiosity as they peer outward. Delicate beaks, one black and one slightly paler, peek out from beneath their fluffy feathers. Surrounding them, slender stems and dried blooms shape a tranquil refuge that cradles these siblings. The scene captures a tender moment of close companionship, as they huddle together for warmth and security amidst the gentle glow of late afternoon."

- "Object Count Consistency": "Verify that exactly two fledgling owls are present." ✗
- "Object Placement and Spatial Reasoning": "Verify that the two owls are nestled side by side within a bed of dried grasses and twigs." ✗
- "Attribute Accuracy": "Verify that each owl's downy plumage is mottled with white speckles atop a warm brown base." ✓
- "Attribute Accuracy": "Verify that each owl has large luminous eyes rimmed in gold and encircled by soft facial discs." ✓
- "Attribute Accuracy": "Verify that one owl's beak is black and the other's is slightly paler." ✗
- "Action Accuracy": "Verify that the owls are huddled closely together to reflect companionship and warmth." ✓
- "Scene Coherence": "Verify that the background includes dried grasses, twigs, slender stems, and dried blooms in a meadow setting." ✓
- "Object Placement and Spatial Reasoning": "Check that surrounding grasses, stems, and dried blooms gently cradle and frame the owls." ✓
- "Scene Coherence": "Verify that warm sunlight filters through tall meadow stalks, producing a gentle late-afternoon glow and natural shadows." ✓
- "Attribute Accuracy": "Confirm that the owls' facial expressions convey curiosity as they peer outward." ✓

Figure 7. Visualization of our rubric based reward. For each prompt, we generate evaluation key-criterion rubrics and score the generated rollout (image) per criteria.